Submitted to

International Europhysics Conference on High Energy Physics, July 12, 2001, Budapest
EPS 2001: Abstract: **787,803**
Parallel Session **Hard High Energy QCD and Structure Functions**

XX International Symposium on Lepton and Photon Interactions, July 23, 2001, Rome
LP 2001: Abstract: **481,496**
Parallel Session **8**

www-h1.desy.de/h1/www/publications/conf/conf_list.html

Inclusive Measurement of Deep Inelastic Scattering at high Q^2 in ep Collisions at HERA

H1 Collaboration

Abstract

The inclusive e^+p single and double differential cross-sections for neutral and charged current processes are measured with the H1 detector at HERA. The data were taken in 1999 and 2000 at a centre-of-mass energy of $\sqrt{s} = 320$ GeV and correspond to an integrated luminosity of $45.9\ \mathrm{pb}^{-1}$. The cross-sections are measured in the range of four-momentum transfer squared Q^2 between 150 and $30\,000$ GeV^2, and Bjorken x between 0.0032 and 0.65. These are compared to previous H1 results based on $35.6\mathrm{pb}^{-1}$ of data taken in 1994 to 1997 at $\sqrt{s} = 300$ GeV. The new measurements are found to be fully consistent with previous ones and well described by next-to-leading order QCD fits in the framework of the Standard Model. In addition the neutral current analysis is extended to small energies of the scattered electron and therefore to values of Bjorken y upto 0.9 allowing a determination of the longitudinal structure function F_L for the first time at high Q^2. The analysis is performed on both the e^+p data, and $16.4\ \mathrm{pb}^{-1}$ of e^-p taken in 1998 and 1999 and F_L is found to be independent of lepton beam.

1 Introduction

Inclusive Deep Inelastic Scattering (DIS) cross-sections are sensitive to the proton structure and QCD dynamics. Since 1992 the experiments H1 and ZEUS have used the colliding lepton–proton beams of the HERA accelerator to extend considerably the phase space of such measurements into new kinematic regions of large four-momentum transfer squared, Q^2, and small x, where x is the Bjorken scaling variable. The large integrated luminosity collected by the experiments has allowed measurements to be made in the very high Q^2 range up to $30\,000$ GeV^2. In this region where $Q^2 \simeq M_Z^2$ or M_W^2, the Z^0 and $W^\pm$ boson masses squared, the effects of the electroweak sector of the Standard Model can be tested in DIS. In addition signals of new physics beyond the Standard Model may be expected to arise at the highest Q^2 where the smallest distance scales of proton structure are probed.

Both contributions to DIS, neutral current (NC) interactions, $ep \to eX$, and charged current (CC) interactions, $ep \to \nu X$ can be measured at HERA and give complementary information on the QCD and electroweak parts of the Standard Model. The cross-sections are defined in terms of two of the kinematic variables Q^2, x, and y, where y quantifies the inelasticity of the interaction.

Measurements of the NC and CC cross-sections in e^+p scattering have been made by H1 and ZEUS based on the data taken in 1994 to 1997 [1, 2] when the ep centre-of-mass energy $\sqrt{s}$ was about 300 GeV. In 1998 and 1999 HERA operated with an electron beam, and the proton beam energy was increased from 820 GeV to 920 GeV ($\sqrt{s} \simeq 320$GeV). H1 collected 16pb^{-1} of e^-p data which was analysed and used together with the e^+p data to extract the structure function $x\tilde{F}_3$ [3]. Here, new e^+p NC and CC cross-section measurements based on data taken at a centre-of-mass energy of 320 GeV in 1999 and 2000 are presented. The luminosity of this data set is 45.9 pb^{-1}.

The new data are compared to those from 1994-1997. In particular the region of high Q^2 is interesting since a slight excess of NC events over the Standard Model expectation was observed in 1994 to 1996 for $Q^2 > 15\,000$ GeV^2 [4, 5]. The NC and CC cross-sections in 1999-2000 are combined with the data from 1994-1997 taking into account the difference in centre-of-mass energy. The measurements are compared to the Standard Model expectations.

Additionally the NC analysis is extended to higher y for $Q^2 < 890$ GeV^2. This extension of the kinematic range allows a determination of the longitudinal structure function, F_L(x,Q^2), to be made at high Q^2 in a region where the influence of $x\tilde{F}_3$ is expected to be negligible. This analysis is performed on both the 1999/2000 e^+p data and the 1998/1999 e^-p data set. The later data have not been reported on in [3].

2 Neutral and Charged Current Cross-Sections

The NC cross-section for the process $e^+p \to e^+X$ with unpolarised beams is given by

$$\frac{\mathrm{d}^2\sigma_{NC}}{\mathrm{d}x\,\mathrm{d}Q^2} = \frac{2\pi\alpha^2}{xQ^4}\left[Y_+\tilde{F}_2 - Y_-x\tilde{F}_3 - y^2F_L\right] \quad , \tag{1}$$

where α is the fine structure constant taken to be $\alpha \equiv \alpha(Q^2 = 0)$ and the helicity dependencies of the electroweak interactions are contained in the functions $Y_\pm \equiv 1 \pm (1-y)^2$. The dominant contribution to the cross-section comes from the generalised structure function $\tilde{F}_2$. The F_L contribution is largest at high y and is expected to diminish with increasing Q^2, whereas the structure function $x\tilde{F}_3$ contributes in the high Q^2 regime of Z^0 exchange.

It is convenient to make use of the NC "reduced cross-section" in which the Q^2 dependence due to the photon propagator is removed

$$\tilde{\sigma}_{NC}(x, Q^2) \equiv \frac{1}{Y_+} \frac{Q^4\, x}{2\pi\alpha^2} \frac{\mathrm{d}^2\sigma_{NC}}{\mathrm{d}x\mathrm{d}Q^2} \quad . \tag{2}$$

Only at high y and high Q^2 do the contributions from F_L and $x\tilde{F}_3$ become important. In these regions the reduced cross-section differs for different centre-of-mass energies while in most of the kinematic range it is independent of the beam energies.

The leading order double differential CC cross-section for $e^+p \to \nu X$ can be written as

$$\frac{\mathrm{d}^2\sigma_{CC}}{\mathrm{d}x\ \mathrm{d}Q^2} = \frac{G_F^2}{2\pi x} \left(\frac{M_W^2}{M_W^2 + Q^2}\right)^2 x\left[(\bar{u} + \bar{c}) + (1-y)^2(d+s)\right] \quad , \tag{3}$$

where G_F is the Fermi coupling constant, and $\bar{u}$, $\bar{c}$, d, s are the quark distributions. The CC reduced cross-section is defined as

$$\tilde{\sigma}_{CC}(x, Q^2) \equiv \frac{2\pi x}{G_F^2} \left(\frac{M_W^2 + Q^2}{M_W^2}\right)^2 \frac{\mathrm{d}^2\sigma_{CC}}{\mathrm{d}x\mathrm{d}Q^2} \quad . \tag{4}$$

3 Experimental Technique

3.1 Detector and Kinematic Reconstruction

The H1 detector is described in detail elsewhere [6]. The co-ordinate system of H1 defines the positive z axis to be in the direction of the incident proton beam. The polar angle θ is then defined with respect to this axis. The forward direction is the region of increasing z.

In order to determine acceptance corrections and background contributions for the DIS cross-section measurements, the detector response to events produced by various Monte Carlo generation programs is simulated in detail, and is described in ref. [1]. The present analysis closely follows that of ref. [1]. The NC event kinematics in the standard analysis are reconstructed using the energy and polar angle of the scattered electron, E_e' and θ_e respectively. The total $E - p_z$ of the event is then obtained from the relation $E - p_z = \Sigma + E_e'(1 - \cos\theta_e)$. Here $\Sigma = \sum_i (E_i - p_{z,i})$, where the summation is performed over all hadronic final state particles. These quantities are used to determine the kinematic variables x, Q^2 , and y in the $e\Sigma$ method [7]:

$$y_{e\Sigma} = 2E_e \frac{\Sigma}{(E - p_z)^2} \qquad Q^2_{e\Sigma} = \frac{P_{T,e}^2}{1 - y_e} \qquad x_{e\Sigma} = \frac{P_{T,e}^2}{s\ y_\Sigma(1 - y_\Sigma)} \quad , \tag{5}$$

where E_e is the incident electron beam energy, and

$$y_\Sigma = \frac{\Sigma}{E - p_z} \qquad y_e = 1 - \frac{E_e^{'}(1 - \cos\theta_e)}{2\ E_e} \qquad P_{T,e} = E_e^{\prime} \sin\theta_e \quad . \tag{6}$$

At high y the kinematic variables are best determined using information from the scattered lepton alone. Therefore, in the *extended analysis* the event kinematics are reconstructed using the electron method (e-method) where

$$Q_e^2 = 4E_e^{'} E_e \cos^2\frac{\theta_e}{2} \qquad x_e = \frac{Q_e^2}{s y_e} \tag{7}$$

and $\sqrt{s}$ is the centre-of-mass energy.

The resolution of both reconstruction methods is controlled by requiring the purity and stability of any x, Q^2 bin to be larger than 30%. The stability (purity) is defined as the fraction of events which originate from a bin and which are reconstructed in it, divided by the number of generated (reconstructed) events in that bin.

The CC event kinematics can only be determined with the hadron method (h method) [8]. The h method kinematic variables are reconstructed using the relations

$$y_h = \frac{\Sigma}{2\ E_e} \qquad Q_h^2 = \frac{P_{T,h}^2}{1 - y_h} \qquad x_h = \frac{Q_h^2}{s\ y_h} \quad , \tag{8}$$

where $P_{T,h} = \sqrt{(\sum_i p_{x,i})^2 + (\sum_i p_{y,i})^2}$ and is summed over all particles of the hadronic final state. This method is influenced by particle losses in the beam pipe and fluctuations of the detector response to hadronic final state particles, and therefore has moderate precision.

3.2 Measurement Procedure

High Q^2 NC events are selected by requiring that the event has a compact electromagnetic cluster, taken to be the scattered electron, in addition to a vertex position within ± 35 cm of its nominal position. The cluster is validated by requiring that an extrapolated track have a distance of closest approach to the cluster of less than 12 cm. This loose cluster-track matching requirement is only applied for $\theta_e \geq 40°$, where θ_e is the polar angle of the scattered electron. In this analysis the polar angle is determined using the position of the electromagnetic cluster and assigned a systematic uncertainty of 3 mrad. The energy of the cluster, $E_e^{\prime}$, is required to be larger than 11 GeV where the trigger efficiency is greater than 99.5%. The total $E - P_z$ summed over all particles is required to be larger than 35 GeV to reduce the photo-production background, and the influence of QED radiative corrections to the measured cross-sections. Fiducial cuts are also made to remove local regions where the electromagnetic shower of the scattered electron is not fully contained in the calorimeter, and where the trigger is not fully efficient. Since the signal to background ratio is reduced in the region of high y, a further kinematic cut is made requiring $y_e \leq 0.9$. The remaining photo-production contribution to the NC cross-sections is never more than 5% at the highest y and negligible elsewhere. The double differential NC reduced cross-section data have a statistical precision of $\sim$ 2% at low Q^2 compared to a total systematic uncertainty of $\sim 4\%$. At the highest x the statistical error increases to about 20% and the systematic errors to about 10%. The total uncertainty is dominated by the statistical error for $Q^2 > 1\,000$ GeV^2. The final sample of selected data consists of about $130\,000$ events. The comparison of the data and the simulation is shown in fig.1 for the scattered electron energy spectrum, and the polar angle θ_e. Both distributions are well described by the simulation.

In 1998 the LAr calorimeter electronics were upgraded allowing the possibility to trigger on scattered leptons as low as 6 GeV and therefore giving access to the high y kinematic region. An NC *extended analysis* is performed in the region $0.9 > y > 0.63$ and $E_e' > 6$ GeV for $90 < Q^2 < 890$GeV^2. In the lower Q^2 range $y = 0.63$ corresponds to $E_e' = 11$ GeV. At low energies of the scattered lepton the photo-production background plays an increasingly important role. In order to keep this background under control it is suppressed by requiring a well measured track to validate the scattered lepton cluster. The track is furthermore required to have the same charge as the beam lepton. Finally, the remaining background is statistically subtracted using fake leptons with the wrong charge as described in [9]. The charge symmetry between right and wrong charge lepton candidates in the background was found to be unity within 10%, and was taken into account in the systematic uncertainties.

In total $24\,000$ e^+p events and $5\,000$ e^-p events are selected in the *extended analysis*. Fig. 2 shows the scattered lepton energy spectrum, the polar angle distribution, and the $E - P_z$ spectrum for the positron data set. The simulation provides a good description of both the e^+p and the e^-p data. F_L is determined from the measured reduced cross-sections using the formula:

$$F_L = \frac{Y_+}{y^2}\left[\tilde{F}_2 - A\tilde{\sigma}_{NC}(x, Q^2)\right], \tag{9}$$

where $\tilde{F}_2$ is taken from the H1 97 PDF Fit. The factor A in the formula accounts for the relative normalisation of the data with respect to the H1 97 PDF Fit (which does not include this data). This factor was obtained by normalising the measured cross-sections in the region $y < 0.4$ with respect to the prediction of the QCD fit. The factors A are found to be 0.99 and 1.00 for the e^-p and e^+p data respectively. The positron data set have a statistical precision on F_L of between 7% and 40% and a systematic uncertainty which ranges between 25% and 50%.

The selection of CC events is based on the expectation that such events have a large missing transverse momentum, $P_{T,h}$, assumed to be carried by an unseen neutrino. Therefore a requirement that $P_{T,h} \geq 12$ GeV is made. In addition the event must have a reconstructed vertex within ± 35 cm of its nominal position. The non-ep and ep background is rejected using the same method as detailed in [1]. The remaining ep background is dominantly due to photo-production events and is negligible for most of the measured kinematic domain, though it may reach up to 3% at $Q^2 = 500\,\mathrm{GeV}^2$. The contribution is subtracted statistically from the CC data sample with a systematic uncertainty of 30% of the subtracted events. In order to restrict the measurement to a region where the kinematic reconstruction is optimal the events are required to have $y_h < 0.85$. The CC trigger efficiency is determined using NC events in which all information associated to the scattered electron is suppressed. This method gives a precise measure of the efficiency which is found to be 78% at $Q^2 = 500\,\mathrm{GeV}^2$ and reaches 99% at $Q^2 = 5000\,\mathrm{GeV}^2$. The measurement is restricted to the region where the trigger efficiency is acceptable by demanding $y_h > 0.03$. After all selection criteria are applied, the final CC data sample contains about 1000 events. The data and simulation are compared in fig.3 for the $P_{T,h}$ and y_h spectra. In both cases the simulation gives a good description of the data.

The electromagnetic and hadronic response of the detector is calibrated using NC events similar to the analysis described in [1]. The procedure is found to give good agreement between data and simulation. The systematic uncertainty of the absolute electromagnetic energy scale varies from 1% in the backward region to 3% in the forward region of the calorimeter. For the hadronic energy scale a conservative uncertainty of 3% is assigned.

The selected events are corrected for detector acceptance and migrations using the simulation and converted to bin centred cross-sections using the prediction from the H1 97 PDF Fit [1]. The cross-sections are corrected for the effects of QED radiation.

3.3 Combination with previous measurements

The new data are combined with the previously published 94-97 e^+p data in order to improve the statistical precision which is the dominant error source for $Q^2 > 1\,000$ GeV^2 in the NC cross-section and at all Q^2 in the CC cross-section.

For this combination the 94-97 data are scaled to the new centre-of-mass energy using the prediction from the H1 97 PDF Fit [1]. The combined measurement of any measured cross-section σ_i is given by

$$\sigma_i = \frac{\sigma_{i,820}^{meas} \cdot \mathcal{L}^{820} + \sigma_{i,920}^{meas} \cdot \mathcal{L}^{920}}{\mathcal{L}^{820} \cdot (\sigma_{i,820}^{th}/\sigma_{i,920}^{th}) + \mathcal{L}^{920}} \tag{10}$$

where σ_{i,E_p}^{meas} and σ_{i,E_p}^{th} are the measured and theoretical cross-sections at a proton energy E_p respectively, and $\mathcal{L}^{820}$ and $\mathcal{L}^{920}$ are the luminosities of the respective data sets. The statistical error is determined correspondingly and the systematic error is assumed to be 100% correlated between the two data sets and conservatively taken from the 99-00 data set. These combined data correspond to a luminosity of 81.5 pb^{-1}.

For the NC reduced cross-sections the correction factor for the beam energy is relatively small. For $Q^2 < 5000$ GeV^2 it is only required for the lowest x bins and is always smaller than 2 %. The largest correction of about 10 % is required at the highest Q^2 and low x. For the CC reduced cross-section it varies between 5 % at low Q^2 and 20 % at high Q^2. For the cross-sections $\mathrm{d}\sigma/\mathrm{dQ}^2$ the correction factor is about 5% at low Q^2 and 50% at the highest Q^2.

4 Results

4.1 Cross-section measurement

The reduced e^+p NC cross-section, $\tilde{\sigma}_{NC}$, is shown in fig. 4 where the results from the new measurement at $\sqrt{s} = 320$ GeV are compared to those obtained at $\sqrt{s} = 300$ GeV. Both sets of measurements are seen to provide comparable precision and are found to be fully compatible. Both data sets also agree well with the predictions of the H1 97 PDF Fit which is also shown. This NLO QCD fit was performed on low Q^2 fixed target data from NMC [10] and BCDMS [11] and the previous H1 high Q^2 e^+p data from 1994-1997. It is shown for the two different centre-of-mass energies of the two data sets.

The reduced NC cross-sections measured at $\sqrt{s} = 300$ GeV and $\sqrt{s} = 320$ GeV are shown in fig. 5 as a function of Q^2 for the high x region. The two data sets are found to be in agreement with each other and with the expectation from the H1 97 PDF Fit. Fig.5 also shows the recent H1 measurement at lower Q^2 [12] and the fixed-target data from BCDMS and NMC. The strong scaling violation is observed over more than four orders of magnitude in Q^2. At the highest Q^2 a decrease of the cross-section is expected due to the negative γZ interference in e^+p scattering. This decrease is clearly seen in the data at $x = 0.18$ and $x = 0.25$. At $Q^2 = 20\,000$ GeV^2 and $x = 0.4$ the new data undershoot the expectation from the H1 97 PDF Fit while the measurement in 1994-1997 exceeded the expectation. In fig. 6 the combined results of the data from 1994 to 2000 are shown, where the 300 GeV data have been corrected individually for the change of centre-of-mass energy. The combined result from all e^+p data shows no significant deviation from the expectation.

In fig. 7 the reduced CC cross-section is shown for the new data and the data taken in 1994-1997. These data are consistent within the statistical errors. The kinematic range for the cross-section measurement was slightly extended at high and low x mainly due to an improved trigger efficiency and hadronic calibration. The combined result is shown in fig. 8 and is found to be in good agreement with the theoretical prediction from the H1 97 PDF Fit. The contribution to the CC reduced cross-section from the d-quark density is also shown as given by the fit. This illustrates that the CC cross-section at high x is mainly sensitive to the d quark (see eq. 3). The precision of the CC cross-section at $x = 0.4$ from all data 1994-2000 is about 20 %.

The single differential NC cross-section $\mathrm{d}\sigma/\mathrm{dQ}^2$ for e^+p data is shown[1] in fig.9(a) for $y \leq 0.9$. The new data are compared to the H1 e^+p measurements based on data in 1994-1997 and the H1 97 PDF Fit. The new preliminary cross-sections are higher than the measurement from 1994-1997 due to the increase in centre-of-mass energy.

Figures 9 (b) show the ratios of the measurements to their corresponding Standard Model expectation. The global 1.5 % luminosity uncertainty of the new data is not included in the error bars. The Standard Model uncertainty represents the uncertainty of the expectation due to assumptions made in the H1 97 PDF Fit, as well as the uncertainties of the experimental data entering the fit, and is detailed in [1]. The new data are observed to agree well with the published data. In fig. 9 (c) the ratio of the combined e^+p cross-section from 1994-2000 to the Standard Model are shown and the data exhibit a similar feature as seen in fig. 6.

The Q^2 dependence of the CC cross-section is shown in fig.10(a) and compared to the previous measurements. Again the effect of the increased centre-of-mass energy is seen resulting in a higher cross-section for the new data set. The ratio of data to expectation is shown in fig.10(b) together with the Standard Model uncertainty. The two data sets agree well with each other and

[1]These measured NC cross-sections are corrected for the small effect of the cut $E'_e > 11$ GeV. Similarly the CC cross-sections are corrected for the cuts $0.03 < y < 0.85$.

with the expectation from the Standard Model. The ratio of the combined 94-00 measurement is also shown in fig. 10(c).

The Q^2 dependence of the NC and CC cross-sections are compared in fig. 11 for the combined 94-00 data. At low Q^2 the NC cross-section is about 1000 times larger than the CC cross-section since the CC cross-section is suppressed due to the propagator term in eq. 3. At the highest values of Q^2 they are of similar size as expected from the Standard Model, although in e^+p data the NC cross section remains larger.

In fig.12 the measurements of F_L are shown at fixed $y = 0.75$ for both the e^+p and the e^-p data sets. Both data sets are mutually consistent and in agreement with the QCD fit. The extreme values allowed for F_L ($F_L = 0$ and $F_L = \tilde{F}_2$) are clearly excluded by the data.

4.2 Valence quark distributions at high Q^2 and high x

The new combined e^+p double differential NC and CC cross-sections together with the e^-p NC and CC cross-sections measured previously based on the data taken in years from 1998 to 1999 [13] are used in a new NLO QCD fit to determine the dominant valence quark distributions xu_v and xu_d at high Q^2 and high x. The fit is performed using the NLO DGLAP evolution equations [14] in the $\overline{\mathrm{MS}}$ factorization scheme and treating the heavy flavours as massless quarks. In addition to the two valence quarks, gluon, up-type and down-type sea quarks are parameterised at $Q_0^2 = 15\,\mathrm{GeV}^2$ in an MRS like form $A_q x^{B_q}(1+x)^{C_q}(1+a_q x^{b_q})$ [16] with $b_q = 1/2$ for the valence quarks and $b_q = 1$ for the rest of quark components. The usual sum rules are imposed. In order to have a reliable constraint on the gluon and sea quarks, the new H1 low Q^2 data [12] are also included. The minimum Q^2-cut on the data is $Q^2_{\mathrm{min}} = 20\ \mathrm{GeV}^2$.

The resulting valence quark densities of this fit are shown in fig. 13 labelled "NLO QCD Fit: H1 only" with the estimated uncertainty. The result is compared to other parameterisations MRST [16], CTEQ5 [17], and the previous H1 fit [1] all of which used the fixed target data of BCDMS [11] and NMC [10]. The uncertainty on the parton densities was estimated from the experimental errors on the data following the prescription given in [15]. The relative precision on the u valence varies between 6% for $x = 0.25$ and 10% for $x = 0.65$. The d valence is essentially constrained by the e^+p CC data only and has a precision of about 20%. The fit agrees with the other parameterisations within the errors at all values of x shown for both xu_v and xd_v except for xu_v at $x = 0.65$ where it is $\sim 17\%$ lower than the other parameterisations with little dependence in the range of Q^2 shown. The difference remains within about two standard deviations. The uncertainty on the valence quark densities comes solely from the high Q^2 data as no difference was found in the central value or the uncertainty when raising the Q^2_{min} cut to 200 GeV^2

Also shown in the figure are the valence quark densities determined with the local extraction method which was introduced in the previous publication [1]:

$$xq_v(x,Q^2) = \sigma_{\mathrm{meas}}(x,Q^2)\left(\frac{xq_v(x,Q^2)}{\sigma(x,Q^2)}\right)_{\mathrm{para}}, \qquad (11)$$

where $\sigma_{\mathrm{meas}}(x,Q^2)$ is the measured NC or CC double differential cross-sections, and the second factor on the right-hand-side of the equation is the theoretical expectation from the previous H1 fit [1]. Only those points where the xq_v contribution is greater than 70% of the total cross section are selected. The extracted parton densities are thus rather independent of the theoretical input as the uncertainty on the dominant valence quark contribution and that of the corresponding cross-section largely cancel in the ratio. The extracted valence quark densities combining $\sigma_{\rm NC}^{e^{\pm}p}$ and $\sigma_{\rm CC}^{e^{-}p}$ represent an improved statistical precision of typically 50% and up to 100% at high Q^2 compared to using the 1994 to 1997 e^+p data only. The local measurements are in good agreement with the global fit.

5 Summary

The NC and CC cross-sections have been measured for e^+p scattering at a centre-of-mass energy of $\sqrt{s} \approx 320$ GeV. Standard Model expectations based on the H1 97 PDF Fit to NMC, BCDMS, and H1 94-97 e^+p data [1] are able to provide a good description of all the measured cross-sections. The NC analysis has been extended to higher y allowing, for the first time, F_L to be determined in the region $110 < Q^2 < 700$ GeV^2 at $y = 0.75$ for e^+p and e^-p data. F_L is observed to be consistent for e^+p and e^-p scattering as expected in the Standard Model, which is in agreement with the data.

Comparisons of these cross-sections with the H1 measurements of NC and CC cross-sections in e^+p scattering from 94-97 data which were taken at a centre-of-mass energy of $\sqrt{s} \approx 300$ GeV are made. The influence of the different centre-of-mass energy is seen in the $\mathrm{d}\sigma/\mathrm{dQ}^2$ cross-section which is about 5 % higher at low Q^2 and 50 % at the highest Q^2. This difference is in agreement with the Standard Model expectation.

The double differential NC reduced cross-sections are measured in the Q^2 range $200 \leq Q^2 \leq 30\,000$ GeV^2, and $0.0032 \leq x \leq 0.65$. The new data agree well with the measurements from 94-97.

The double differential CC reduced cross-sections are measured in the Q^2 range $300 \leq Q^2 \leq 15\,000$ GeV^2, and $0.008 \leq x \leq 0.4$. The new data agree well with the theoretical prediction and with the 94-97 measurements. Since the dominating error is statistical for the CC cross-section the precision is improved from about 30 % to 20 % for each data point when combining the 99/00 data with those from 94-97.

A new NLO QCD fit was performed using all available cross-sections measured by H1, but did not include the measurements of F_L. It can be seen for the first time that the valence quark distributions xu_v and xd_v can be separately constrained from the HERA high Q^2 data alone with an experimental precision of about 10% and 20% respectively for xu_v and xd_v at $x = 0.65$ and $x = 0.4$. The u valence quark density at high x is found to be about 17 % lower than other parameterisations using the fixed target data. The parton densities determined with the local extraction method are in good agreement with the global QCD fit.

Acknowledgments

We are grateful to the HERA machine group whose outstanding efforts have made and continue to make this experiment possible. We thank the engineers and technicians for their work in constructing and now maintaining the H1 detector, our funding agencies for financial support, the DESY technical staff for continual assistance, and the DESY directorate for the hospitality which they extend to the non-DESY members of the collaboration.

References

[1] H1 Collab., C. Adloff et al., Eur. Phys. J. **C13** (2000) 609-639.

[2] ZEUS Collab., J.Breitweg et al. , Eur. Phys. J. **C11** (1999) 427-445.
ZEUS Collab., J.Breitweg et al. , Eur. Phys. J. **C12** (2000) 411-428.

[3] H1 Collab., C. Adloff et al., Eur. Phys. J. **C19** (2001) 269-288

[4] H1 Collab., C. Adloff et al., Z. Phys. **C74** (1997) 191.

[5] ZEUS Collab., J. Breitweg et al., Z. Phys. **C74** (1997) 207.

[6] H1 Collab., I. Abt et al., *Nucl. Instrum. Methods* **A 386** (1997) 310 and 348.

[7] U. Bassler and G. Bernardi, Nucl. Instr. Meth. **A361** (1995) 197;
U. Bassler and G. Bernardi, Nucl. Instr. Meth. **A426** (1999) 583.

[8] A. Blondel and F. Jacquet, Proceedings of the Study of an ep Facility for Europe, ed. U. Amaldi, DESY 79/48 (1979) 391.

[9] B. Reisert, Ph.D. Thesis, Max-Planck-Institut für Physik,Munich, MPI-PhE/2000-26.
Also available at http://www-h1.desy.de/publications/theses_list.html

[10] NMC Collab., M. Arneodo et al., Phys. Lett. **B364** (1995) 107.

[11] BCDMS Collab., A.C. Benvenuti et al., Phys. Lett. **B223** (1989) 485.

[12] H1 Collab., Conf. Paper 944, 30th Intern. Conf. on High-Energy Physics, Osaka, Japan (2000), July 2000

[13] H1 Collab., Conf. Paper 971, 30th Intern. Conf. on High-Energy Physics, Osaka, Japan (2000), July 2000

[14] L. N. Lipatov, *Sov. J. Nucl. Phys.* **20** (1975) 95; V. N. Gribov and L. N. Lipatov, *Sov. J. Nucl. Phys.* **15** (1972) 438; G. Altarelli and G. Parisi, *Nucl. Phys.* **B126** (1977) 298; Yu. L. Dokshitzer *Sov. Phys. JETP* **46** (1977) 641.

[15] C. Pascaud and F. Zomer, LAL preprint, LAL/95-05 (1995)

[16] A. D. Martin *et al.*, *Eur. Phys. J.* **C4** (1998) 463; hep-ph/9803455.

[17] See e.g. CTEQ Collab., H. L. Lai *et al.*, *Phys. Rev.* **D**55 (1997) 1280; hep-ph/9701256, hep-ph/9903282.

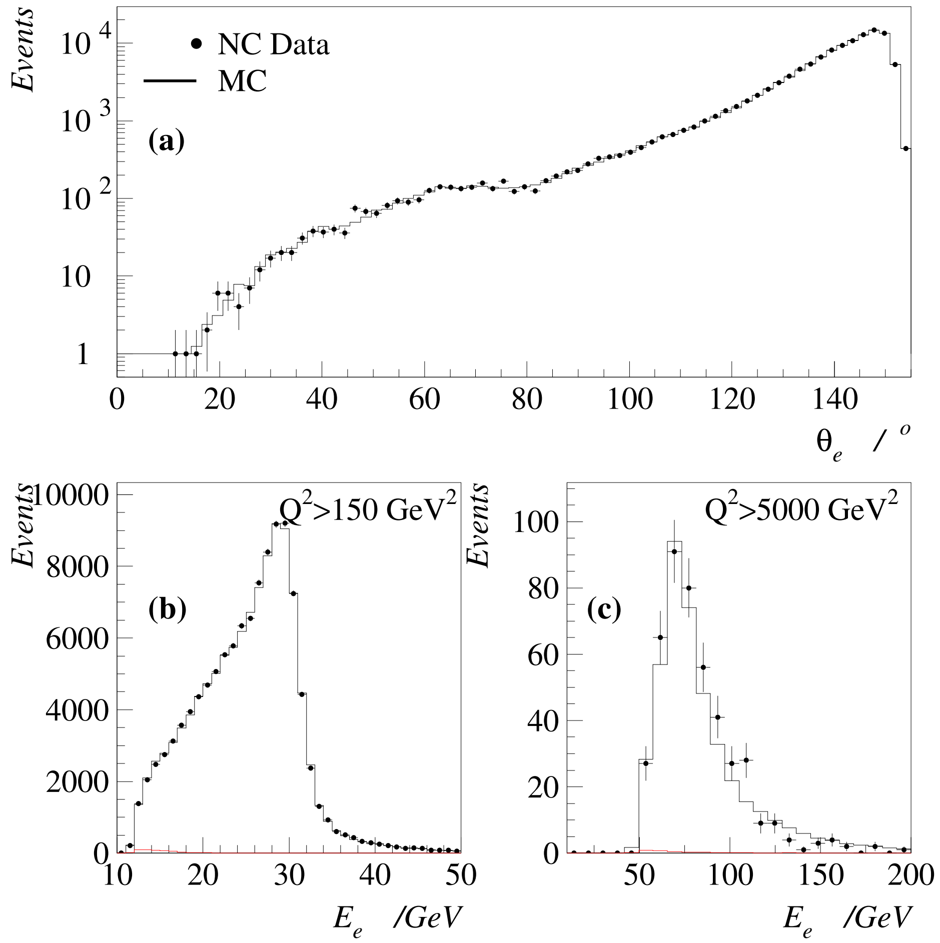

Figure 1: Distributions of (a) θ_e and E_e' for (b) $Q^2 > 150$ GeV^2 and (c) $Q^2 > 5000$ GeV^2 (solid points) and simulation (solid line) for e^+p data. The lower histograms show the photoproduction contribution.

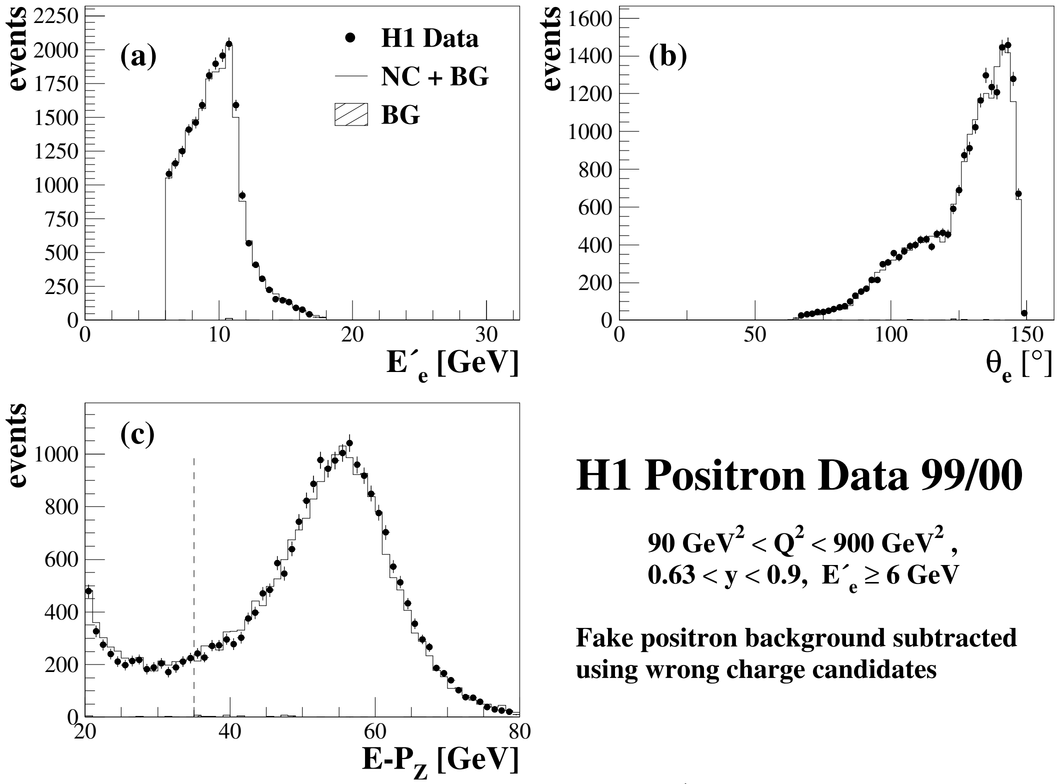

Figure 2: Distributions of (a) E'_e, (b) θ_e and (c) $E - P_z$ for e^+p data (solid points) and simulation (solid line) in the *extended analysis*.

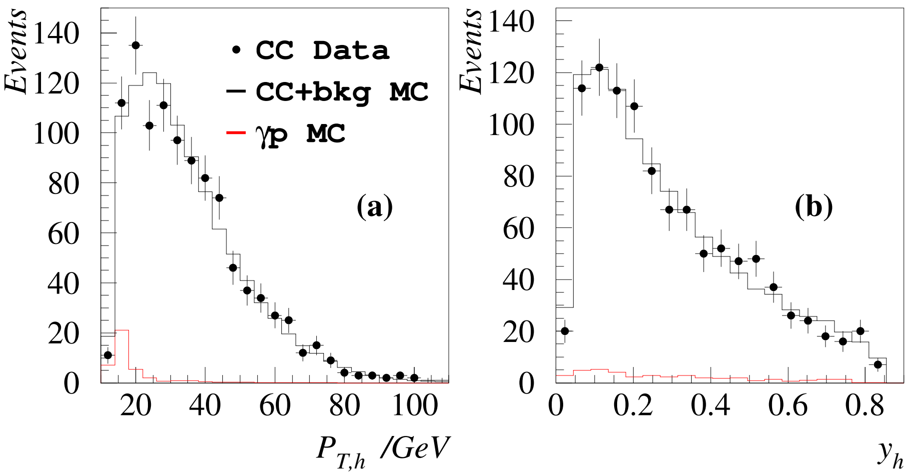

Figure 3: Distributions of (a) $P_{T,h}$ and (b) y_h for CC data (solid points) and simulation (solid line). The lower histograms show the photo-production contribution.

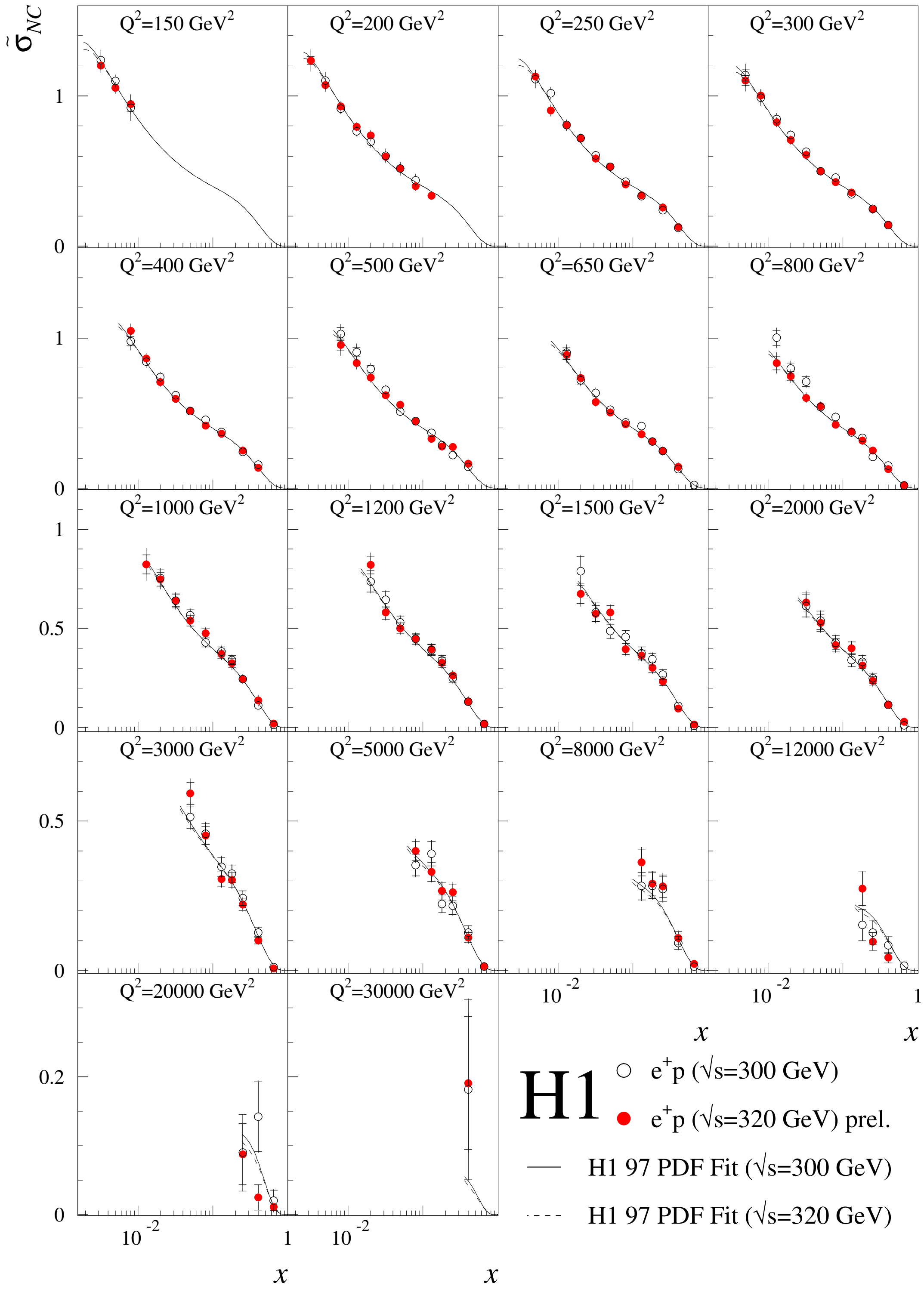

Figure 4: The NC e^+p reduced cross-section $\tilde{\sigma}_{NC}$ is compared to the H1 97 PDF Fit. The 99-00 and the 94-97 measurements are shown with the H1 97 PDF Fit predictions for the different centre-of-mass energies. The inner error bars represent the statistical error, and the outer error bars show the total error.

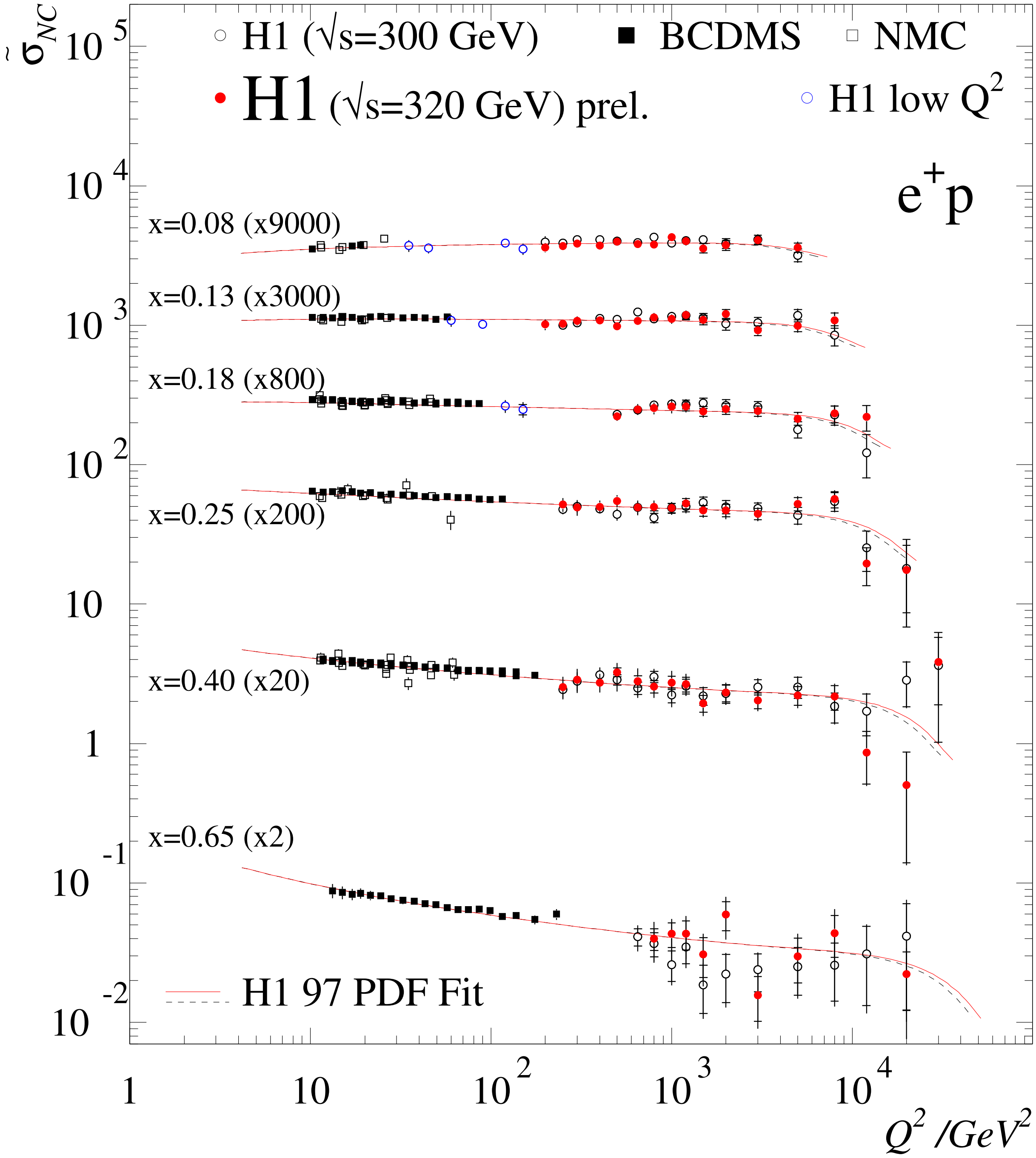

Figure 5: The NC reduced cross-sections $\tilde{\sigma}_{NC}$ from the 94-97 and 99-00 data are shown at high x compared to the H1 97 PDF Fit. Also shown are data from the H1 measured at lower Q^2, as well as fixed-target experiments BCDMS and NMC. The solid (dashed) curve represents the Standard Model expectation based on the H1 97 PDF Fit for $\sqrt{s} = 320$ GeV ($\sqrt{s} = 300$ GeV). The inner error bars represent the statistical error, and the outer error bars show the total error.

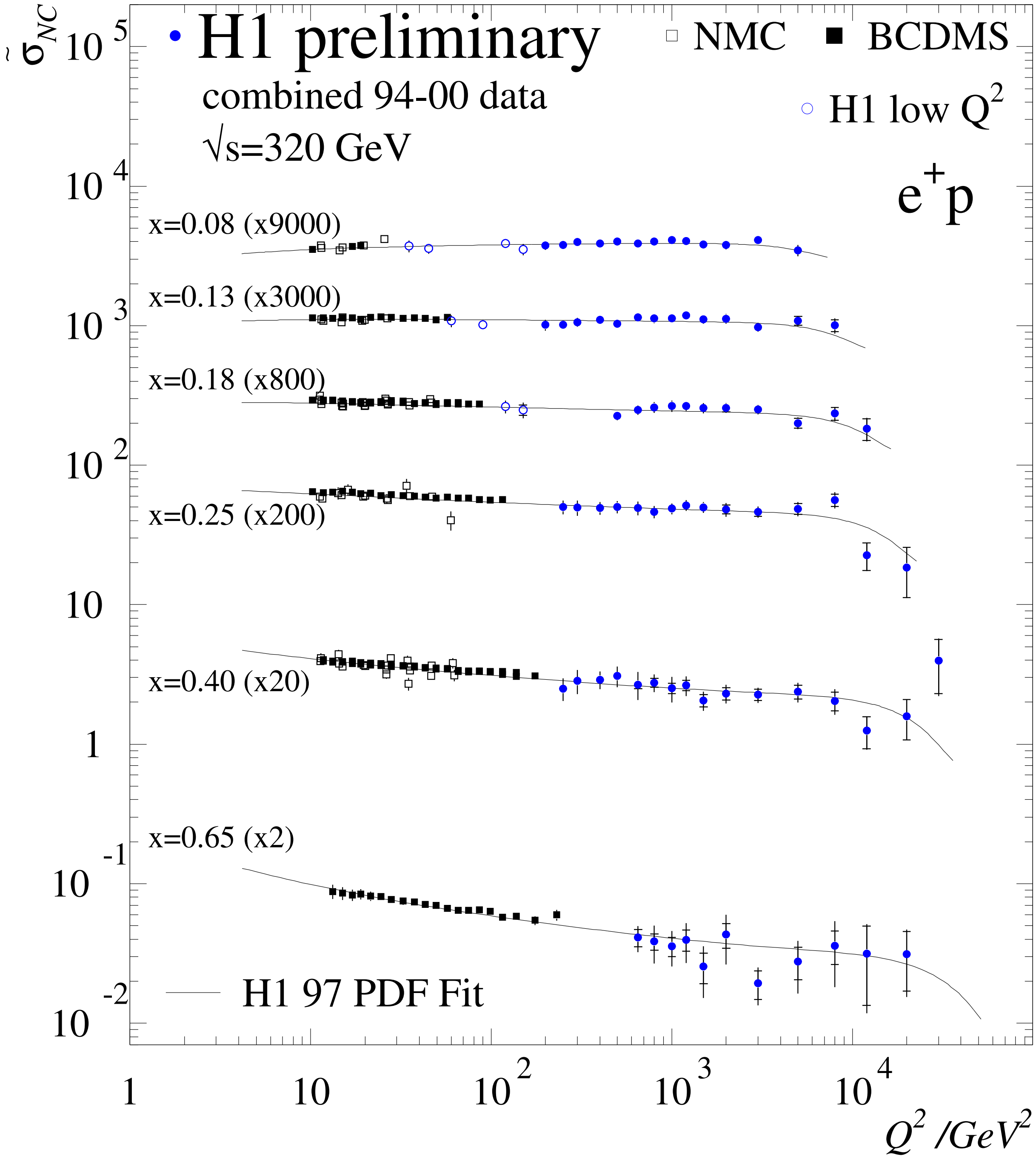

Figure 6: The NC reduced cross-section $\tilde{\sigma}_{NC}$ from the combined 94-00 data is shown at high x compared to the H1 97 PDF Fit. Also shown are data from the fixed-target experiments BCDMS and NMC. The solid curves represent the Standard Model expectation based on the H1 97 PDF Fit. The inner error bars represent the statistical error, and the outer error bars show the total error.

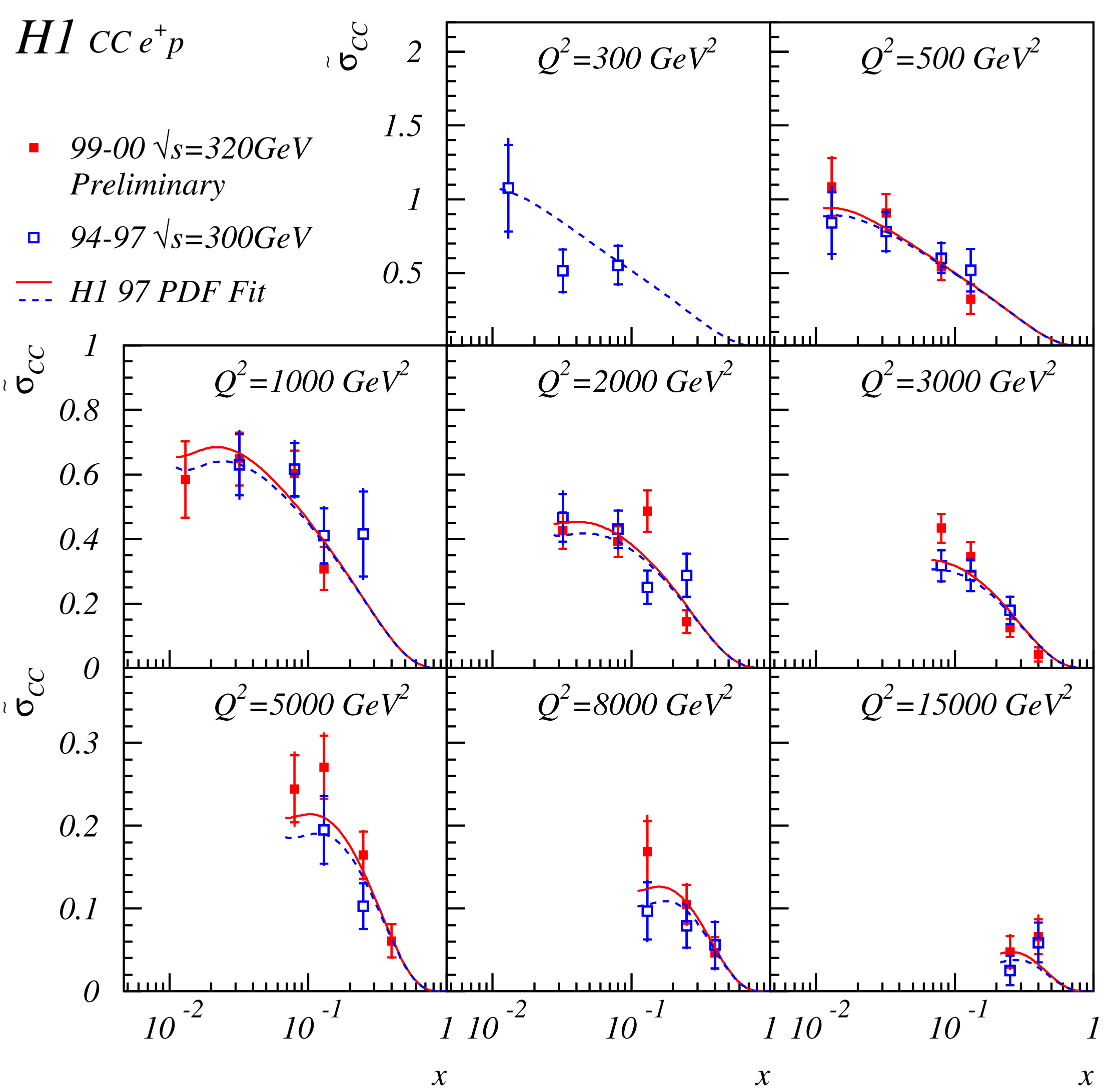

Figure 7: The CC reduced cross-section $\tilde{\sigma}_{CC}(x, Q^2)$ is shown for e^+p scattering for the new data from 1999-2000 at $\sqrt{s} \approx 320$ GeV (solid squares) and the data from 1994-1997 at $\sqrt{s} \approx 300$ GeV (open squares). The data are compared to the H1 97 PDF Fit with the full and dashed curves showing respectively for $\sqrt{s} \approx 320$ GeV and $\sqrt{s} \approx 300$ GeV. The full line refers to the H1 97 PDF Fit and the dashed curve indicates the d contribution in that model. The inner error bars represent the statistical error, and the outer error bars show the total error.

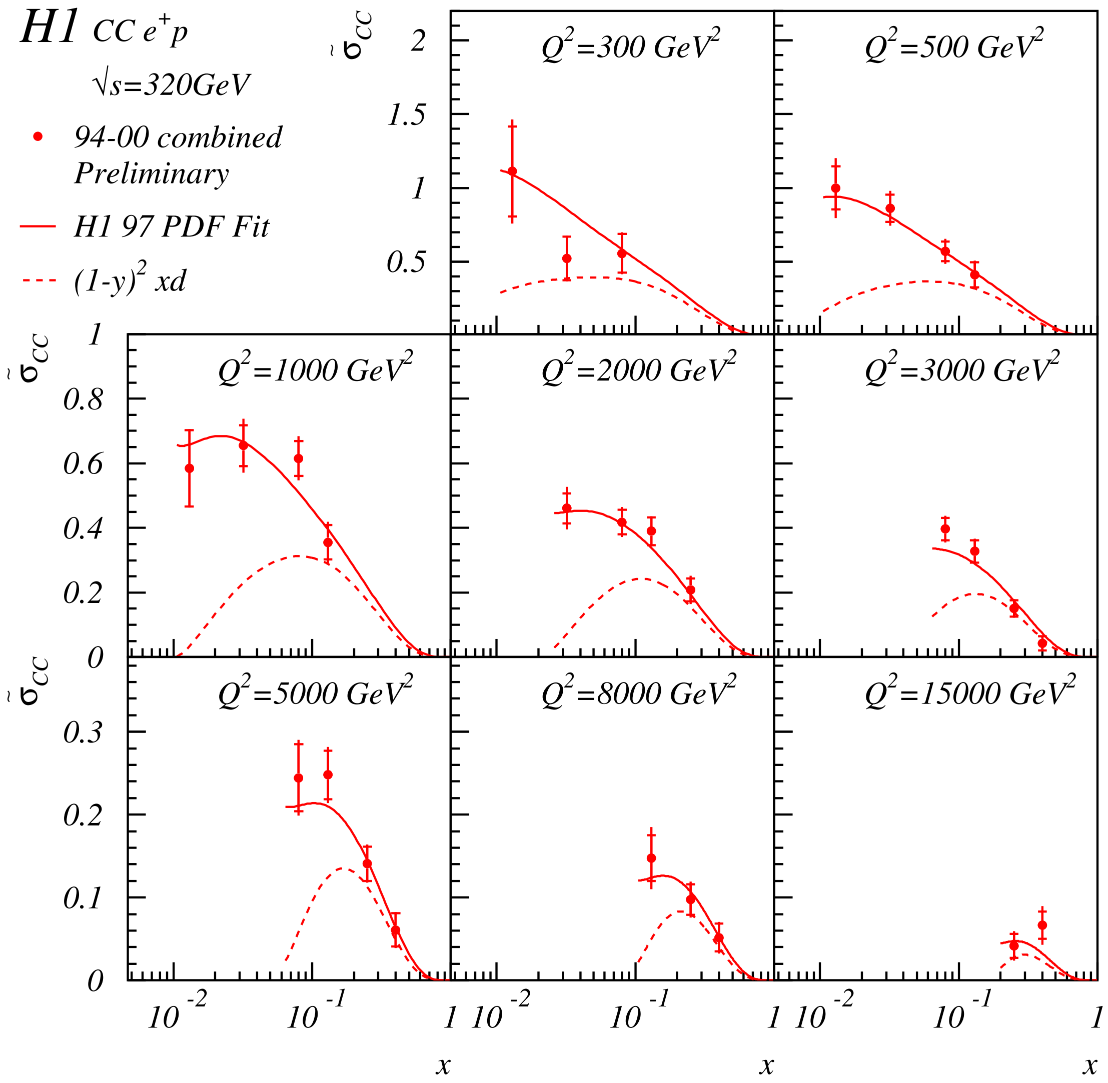

Figure 8: The CC reduced cross-section $\tilde{\sigma}_{CC}(x, Q^2)$ for e^+p scattering is shown for the combined data from 94-00 at $\sqrt{s} \approx 320$ GeV. The data are compared to the H1 97 PDF Fit. The inner error bars represent the statistical error, and the outer error bars show the total error.

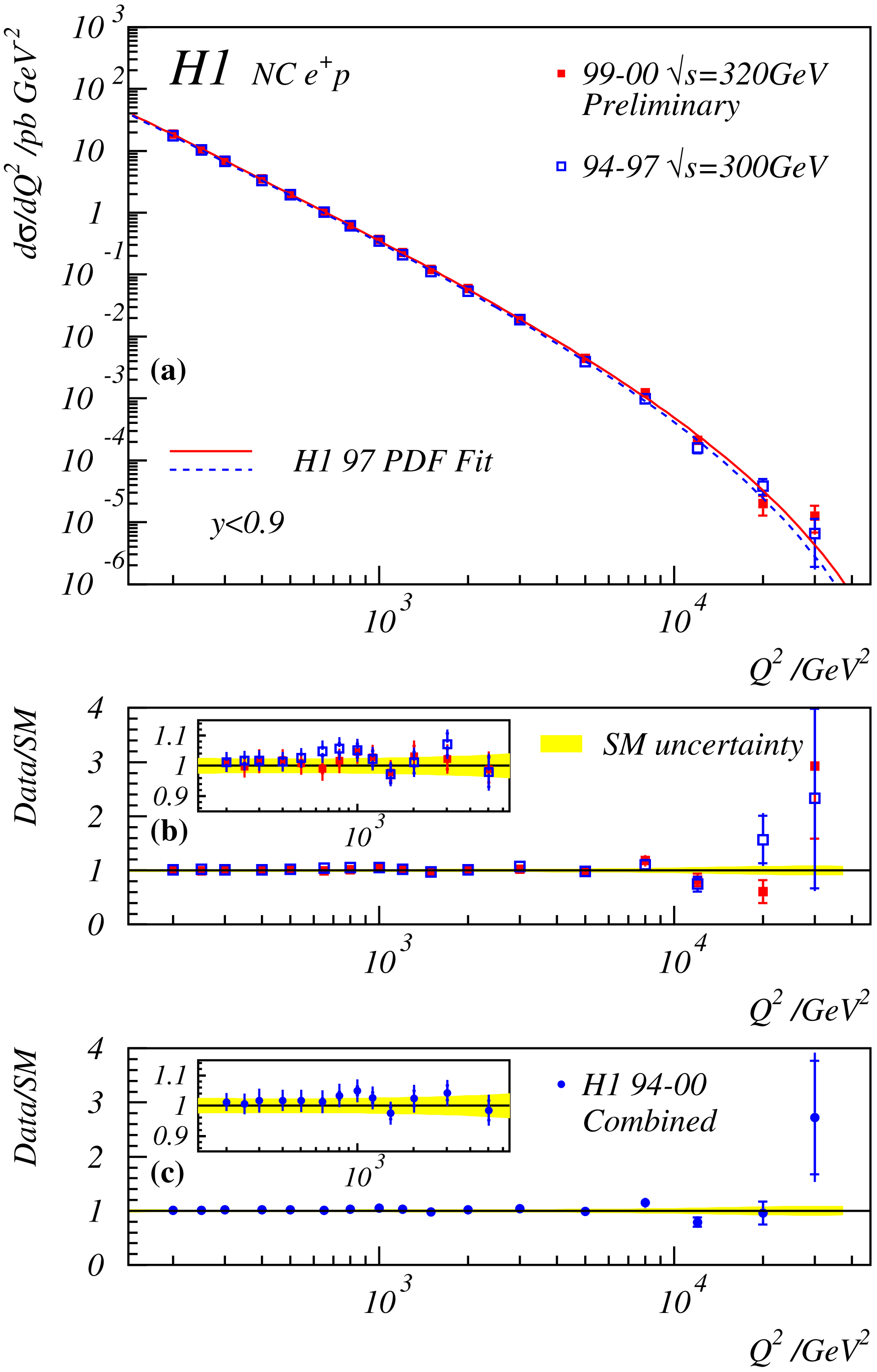

Figure 9: The Q^2 dependence of NC cross-sections $d\sigma/dQ^2$ is shown for the new preliminary e^+p (solid points) and published 94-97 e^+p (open points) measurements. The data are compared to the Standard Model expectation determined from the H1 97 PDF Fit. The dashed (full) line corresponds to a center-of-mass energy of $\sqrt{s} = 300$ GeV ($\sqrt{s} = 320$ GeV). The ratio of the 94-97 and 99-00 data to their respective Standard Model expectation is shown in figure (b). In fig. (c) the ratio of the combined 94-00 NC cross-section to the Standard Model is shown. The Standard Model Uncertainty is shown as the shaded band. The 1.5% luminosity uncertainty is not included in the error bars.

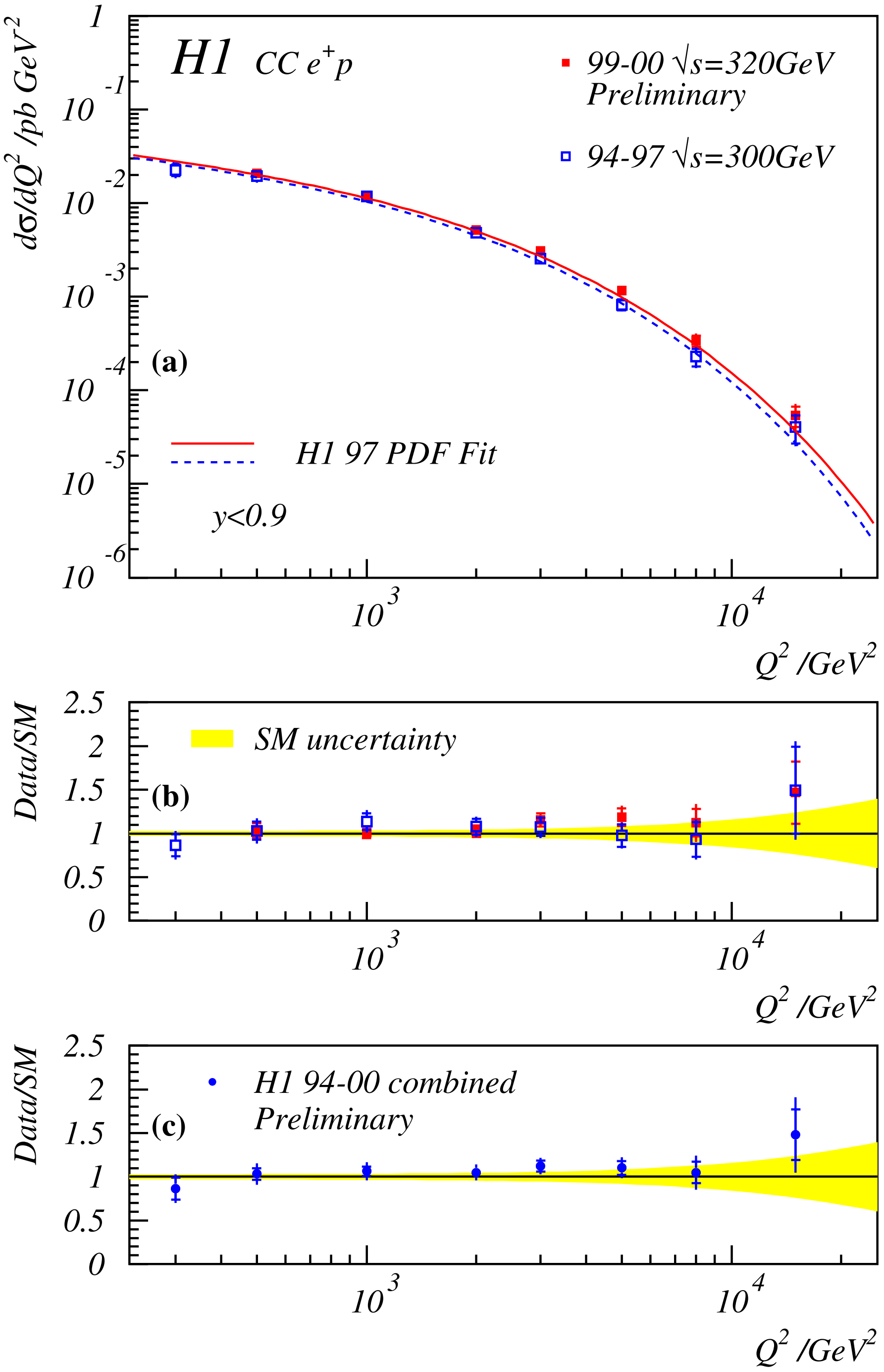

Figure 10: The Q^2 dependence of CC cross-section $d\sigma/dQ^2$ is shown for the new preliminary e^+p (solid points) and published 94-97 e^+p (open points) measurements. The data are compared to the Standard Model expectation determined from the H1 97 PDF Fit. The dashed (full) line corresponds to a center-of-mass energy of $\sqrt{s} = 300$ GeV ($\sqrt{s} = 320$ GeV). The ratio of the 94-97 and 99-00 data to their respective Standard Model expectation is shown in figures (b). In fig. (c) the ratio of the combined 94-00 CC cross-section to the Standard Model is shown. The Standard Model Uncertainty is shown as the shaded band. The 1.5% luminosity uncertainty is not included in the error bars.

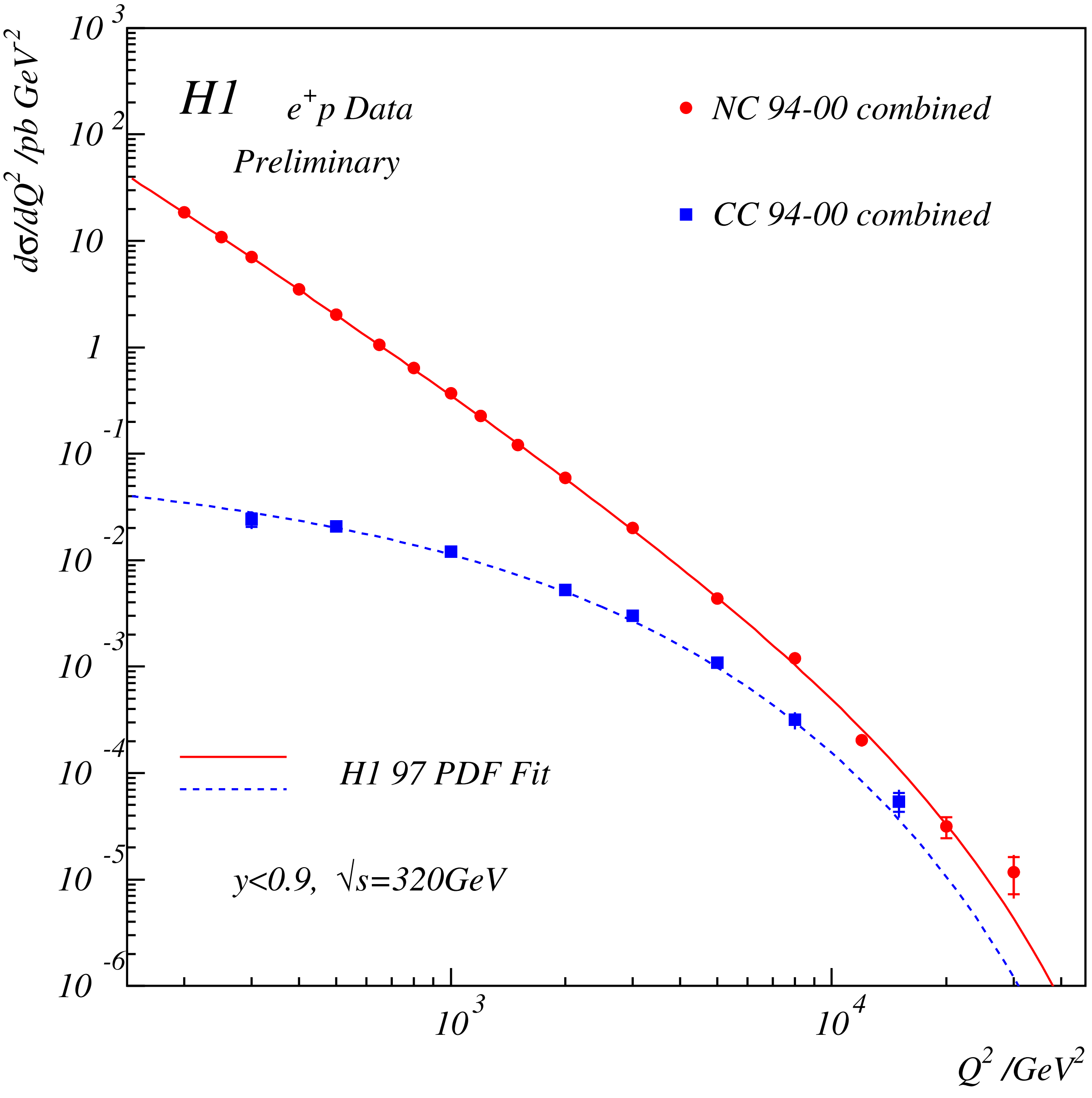

Figure 11: The Q^2 dependence of the NC (circles) and CC (squares) cross-sections $d\sigma/dQ^2$ is shown for the combined 94-00 e^+p measurements. The data are compared to the Standard Model expectations determined from the H1 97 PDF Fit including the 94-97 H1 e^+p data. The 1.5% luminosity uncertainty is not included in the error bars.

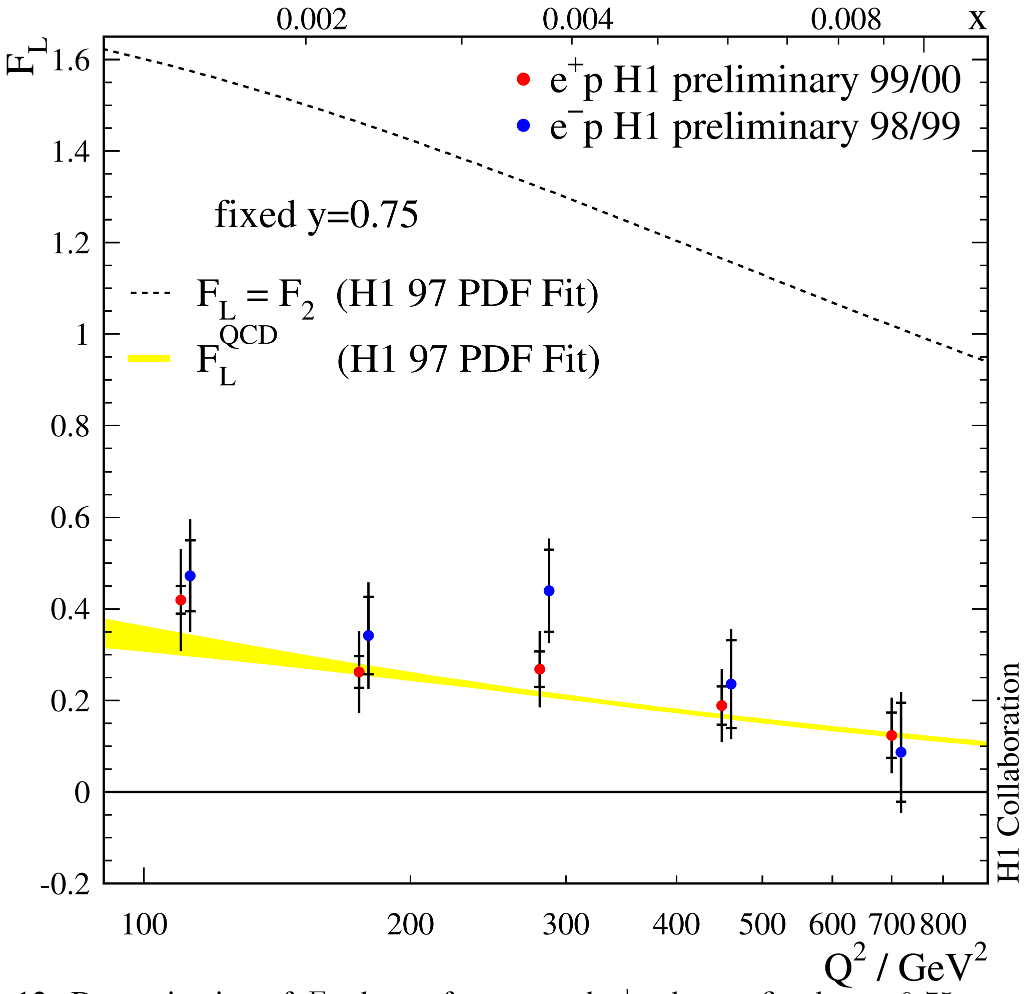

Figure 12: Determination of F_L shown for e^-p and e^+p data at fixed $y = 0.75$ as a function of Q^2 (lower scale), or equivalently x (upper scale). The shaded band shows the expectation of F_L, and its uncertainty, from the QCD fit.

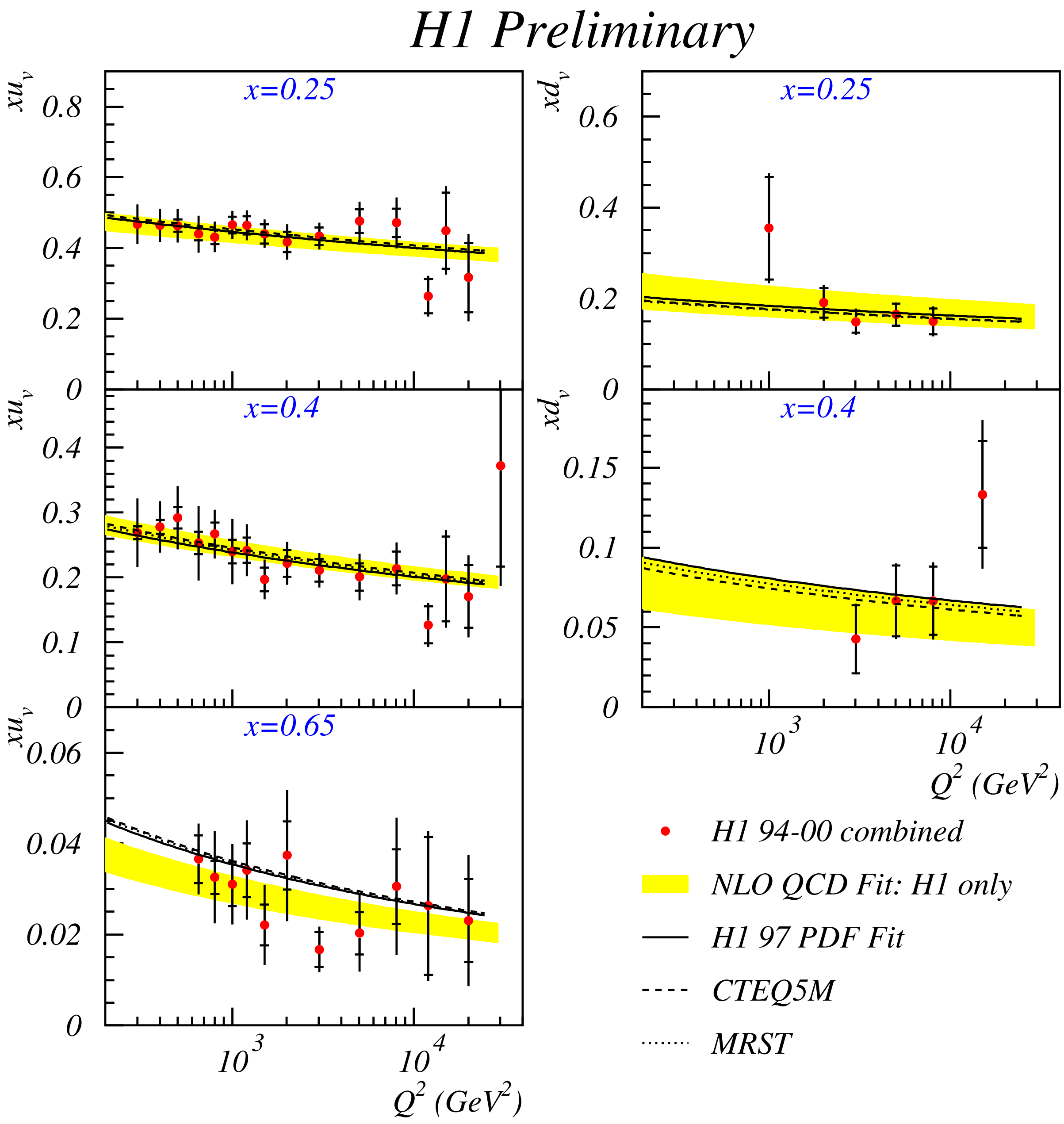

Figure 13: The valence quarks distributions xu_v and xd_v determined both with the NLO QCD fit (shaded error bands) using all cross-section measurements from H1 only and with the local extraction method (data points with the inner and full error bars showing respectively the statistical and total errors) in comparison with other parameterizations which used fixed target data at low Q^2.